

Three-dimensional imaging of skin melanoma *in vivo* by dual-wavelength photoacoustic microscopy

Jung-Taek Oh

Meng-Lin Li

Hao F. Zhang

Konstantin Maslov

Texas A&M University
Department of Biomedical Engineering
Optical Imaging Laboratory
3120 TAMU
College Station, Texas 77843-3120

George Stoica

Texas A&M University
Department of Veterinary Pathobiology
5547 TAMU
College Station, Texas 77843-5547

Lihong V. Wang

Texas A&M University
Department of Biomedical Engineering
Optical Imaging Laboratory
3120 TAMU
College Station, Texas 77843-3120

Abstract. Dual-wavelength reflection-mode photoacoustic microscopy is used to noninvasively obtain three-dimensional (3-D) images of subcutaneous melanomas and their surrounding vasculature in nude mice *in vivo*. The absorption coefficients of blood and melanin-pigmented melanomas vary greatly relative to each other at these two optical wavelengths (764 and 584 nm). Using high-resolution and high-contrast photoacoustic imaging *in vivo* with a near-infrared (764-nm) light source, the 3-D melanin distribution inside the skin is imaged, and the maximum thickness of the melanoma (~0.5 mm) is measured. The vascular system surrounding the melanoma is also imaged with visible light (584 nm) and the tumor-feeding vessels found. This technique can potentially be used for melanoma diagnosis, prognosis, and treatment planning. © 2006 Society of Photo-Optical Instrumentation Engineers. [DOI: 10.1117/1.2210907]

Keywords: medical and biological imaging; photoacoustic imaging; three-dimensional microscopy; spectroscopy; tissue diagnostics.

Paper 06034LR received Feb. 22, 2006; revised manuscript received Apr. 17, 2006; accepted for publication Apr. 17, 2006; published online Jun. 14, 2006.

The incidence of melanoma has increased dramatically worldwide in recent years and poses a major threat to public health. In the USA, the incidence of melanoma is rising faster than any other cancer, with an estimated 20,000 to 40,000 cases of *in situ* cutaneous malignant melanoma (CMM) and 47,700 cases of invasive CMM diagnosed every year.¹ Consequently, there is an increased demand for the development of new clinically related technologies that will allow early diagnosis and accurate prognosis of melanoma.

Knowledge of the depth of invasion and the three-dimensional (3-D) shapes of malignant melanomas are critical to clinical decision-making and prognosis.² The depth and the thickness of the cancerous tissue are particularly important in the choice of treatment. Current clinical practice is based on invasive excisional or incisional biopsies, which are not only accompanied by pain but are also potentially damaging to nearby healthy skin. Noninvasive imaging methods have the potential to eliminate these problems and also to permit the monitoring of treatment effects.

Although several technologies have been previously explored as possible noninvasive melanoma imaging methods, almost all of them suffer from critical limitations. Epithelial illumination microscopy and confocal scanning laser microscopy offer insufficient penetration depth for the measurement of melanoma thickness.^{3,4} High-frequency sonography provides good penetration depth, but the thickness of the melanoma cannot be obtained directly because the image contrast

does not originate from the echo-poor melanoma but from the echo-rich dermis nearby.⁵

Photoacoustic tomography is a new noninvasive imaging modality, and it is emerging as a very practical method for imaging biological tissue structures by means of laser-induced ultrasound.⁶ Structures with high optical absorption, such as blood vessels, can be imaged with the spatial resolution of ultrasound, which is not limited by the strong light scattering in biological tissues. Recently, images of microvasculature as deep as 3 mm were demonstrated with high-resolution photoacoustic microscopy.⁷

In this study, *in vivo* 3-D shapes of subcutaneous melanoma and the nearby vascular system were imaged with the photoacoustic modality. A pair of pulsed lasers was employed to produce light at different wavelengths, thereby differentiating between the contrasts that are due to the absorption of melanin in the melanoma and those that are due to blood in the vessels. Moreover, a dark-field optical illumination, high-numerical-aperture (NA) acoustic lens and a wideband ultrasonic transducer provided high lateral and axial resolution photoacoustic images for both wavelengths. Using high-contrast photoacoustic imaging with a near-infrared (NIR) (764-nm) light source, the 3-D melanin distribution inside the skin was imaged, and the thickness and depth of the melanoma were found accordingly. The vascular system surrounding the melanoma was also visualized with visible light (584 nm).

Figure 1 shows the experimental setup for photoacoustic microscopy. A tunable Ti:sapphire laser (LT-2211A, Lotis) and a tunable dye laser (ND6000, Continuum) were employed

Address all correspondence to Lihong Wang, Biomedical Engineering, Texas A&M University, 3120 TAMU — MS 3120, College Station, TX 77843-3120; Tel: 979 847 9040; Fax: 979-847-4450; E-mail: lwang@tamu.edu

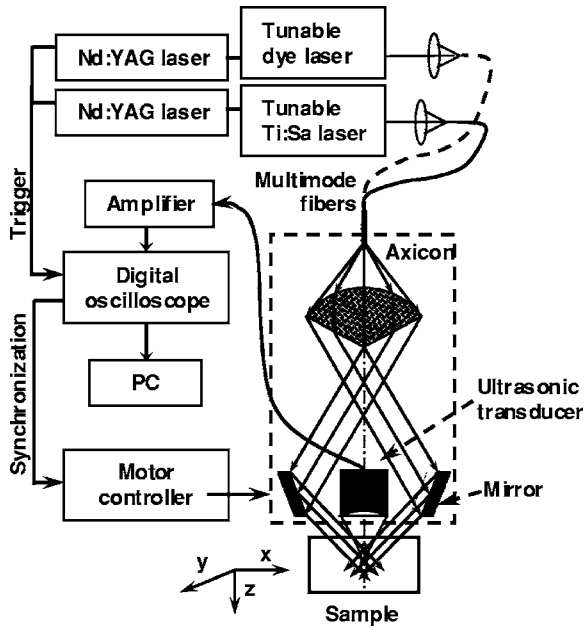


Fig. 1 Schematic of the dual-wavelength photoacoustic microscope for melanoma imaging.

to provide pulses with wavelengths of 764 and 584 nm, respectively. The wavelengths were chosen to maximize the difference between the optical absorption of blood and that of melanin within the tuning range of each laser. The optical absorption coefficients of heavily pigmented skin and blood are known to be 30 to 70 cm^{-1} and $\sim 4 \text{ cm}^{-1}$ for NIR light and 72 to 172 cm^{-1} and $\sim 187 \text{ cm}^{-1}$ for visible light, respectively.⁸ NIR light (wavelength $\lambda = 764 \text{ nm}$) was used to visualize the melanin, while visible light ($\lambda = 584 \text{ nm}$) was selected to visualize the vascular structure. The laser pulse widths for the Ti:sapphire and the dye laser were 15 and 6.5 ns, respectively, and the pulse repetition rate was 10 Hz for both lasers. The laser output was delivered to a multimode fiber with a 0.6-mm core diameter. The tip of the fiber was positioned so as to have a diverging annular beam, focused using a conical lens so that the light focus overlapped with the focus of the high-frequency ultrasound transducer (V214-BC-RM, Panametrics). The incident light energy densities of both the NIR and visible light sources on the sample surface were controlled to be less than 3 and 1 mJ/cm^2 , respectively, which are well within the safety standards.⁹ Dark-field illumination with an incident angle of 45 deg was used to reduce the strong acoustic waves emitted from structures close to the skin and the upper surface of the melanoma, which could potentially overshadow the weaker acoustic waves from deeper structures. An ultrasound transducer with a central frequency of 50 MHz, a nominal bandwidth of 70%, and an NA of 0.44 was used. Owing to the highly optical scattering nature of biological tissue, the characteristics of the detecting transducer determine the resolution of the system. The high NA of the ultrasound transducer provides a lateral resolution of 45 μm and an axial resolution of 15 μm . The photoacoustic signals received by the transducer were amplified and then recorded by a digital oscilloscope. The transducer was immersed in water inside a plastic container with an opening at

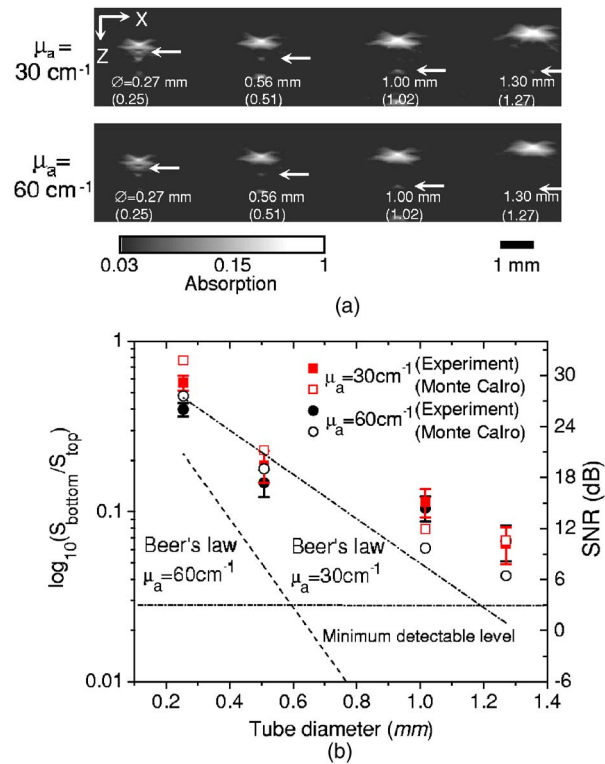


Fig. 2 (a) Maximum thickness measurement test with tubes filled with ink imbedded inside a tissue phantom; the arrows indicate the bottom boundaries of the tubes; ϕ : tube inner diameter. (b) Photoacoustic signal ratio between the top and bottom of the tubes.

the bottom that was sealed with a thin transparent disposable membrane. The animal was placed outside the container below the membrane, and the ultrasonic coupling was further secured by coupling gel. A mechanical stage provided lateral scanning of the photoacoustic sensor, which allowed a cross-sectional B-scan and a planar C-scan over the sample to be obtained. Finally, a synthetic-aperture focusing technique (SAFT) was employed to increase the image resolution at the defocused zone of the transducer.¹⁰

Figure 2(a) shows the cross-sectional (B-scan) NIR photoacoustic images of the melanoma phantoms that were constructed of four different sizes of tubes (inner diameter: 0.25, 0.51, 1.02, and 1.27 mm; Tygon SH-51, Saint-Goban) and filled with ink embedded inside a layer of light diffusing tissue phantom made from a 1%-Intralipid (Liposyn, Abbott Labs) and 10%-porcine gel. The tubes were positioned at a depth of 1.5 mm in the gel phantom. The absorption coefficients of the ink samples for the NIR light source were $\mu_a = 30 \text{ cm}^{-1}$ and 60 cm^{-1} , which are close to the absorption coefficients of the highly melanin pigmented tissues at the wavelength.⁷ The measured absorption coefficient ($\mu_a = 0.27 \text{ mm}^{-1}$) and reduced scattering coefficient ($\mu'_s = 8.4 \text{ cm}^{-1}$) of the tissue phantom are also comparable to those of skin tissue. Each image is a gray-scale plot of the envelope magnitude of the received photoacoustic signals. The envelope peaks were chosen to define the upper and lower boundaries of the embedded tubes. The vertical and the horizontal axes of the images represent the depth from the top surface and the horizontal transducer position, respectively,

and each image has a physical size of 3.0 mm in depth and 14.0 mm in width. The arrows in the figure indicate the bottom boundaries, and the images show that both boundaries are visible up to 1.27 mm of thickness in the melanin phantom. This demonstrates the capability of the current system to detect the thickness of skin melanoma cancer. The numbers below the images are the measured inner diameters which are in good agreement with the real values that are provided in parentheses. Because of ultrasound impedance mismatch between the tube and the ink solution, strong photoacoustic pressure that was generated from the top boundary of the tube reverberated to the bottom boundary. The reverberation signal appeared after a distance exactly equal to two times the tube diameter in the images and was easy to exclude from the experiment.

A quantitative evaluation of the maximum measurable thickness for a melanoma using the photoacoustic microscopy system is shown in Fig. 2(b). The ratio between the experimental photoacoustic signal strength from the upper and lower boundaries of the structure obtained from Fig. 2(a) is compared with the signal ratio from a Monte Carlo simulation based on the optical setup and the theoretical ratio following Beer's law for nonscattering media.¹¹ A linear relationship between the light absorption and the photoacoustic signal was assumed for the simulation. Normalization of the signal from the lower boundary with the upper one permits us to incorporate the signal-to-noise ratio (SNR) into the evaluation of the maximum measurable thickness under the condition that the strong signal from the upper boundary is equal to the maximum signal level of the system. The maximum measurable depth for the two ink samples can be estimated by the extrapolation of the experimental data to the 3-dB signal level as indicated in Fig. 2(b). The maximum measurable thickness for the highest absorption case, $\mu_a=60\text{ cm}^{-1}$, is found to be around 1.5 mm. Although there is some discrepancy between the experimental and Monte Carlo simulation results for dark-field illumination, the experimental data follows the trend of the Monte Carlo simulation results faithfully. It implies that the photoacoustic microscopy signal largely follows the absorption distribution around the sample. As the absorption coefficient increases, the experimental photoacoustic signal decay is much slower as compared to bright-field illumination. It is evident that oblique illumination and light diffusion make the optical fluence at the bottom surface higher while reducing it at the top surface, which finally increases the measurement thickness without overshadowing the weak signal at the bottom. Since the light distribution near the melanoma determines the maximum measurable thickness, for thick melanoma cases, it is necessary to optimize the incident angle of the dark-field illumination and the focal depth.

Immunocompromised nude mice (Harlan Co.) weighing about 20 g were used for the *in vivo* animal experiments. The mice were inoculated with highly invasive B16 skin melanoma cells (ATCC, Manassas, VA, USA) subcutaneously in the upper lumbar area to the left of the vertebra four days before the experiment. Imaging was performed under isoflurane gas anesthesia with a dose of 1% of pure oxygen at a 1 L/min flow rate. The body temperature of the animal was maintained by controlling the temperature of the water in the immersion container to 36°C. The pulse rate and the global

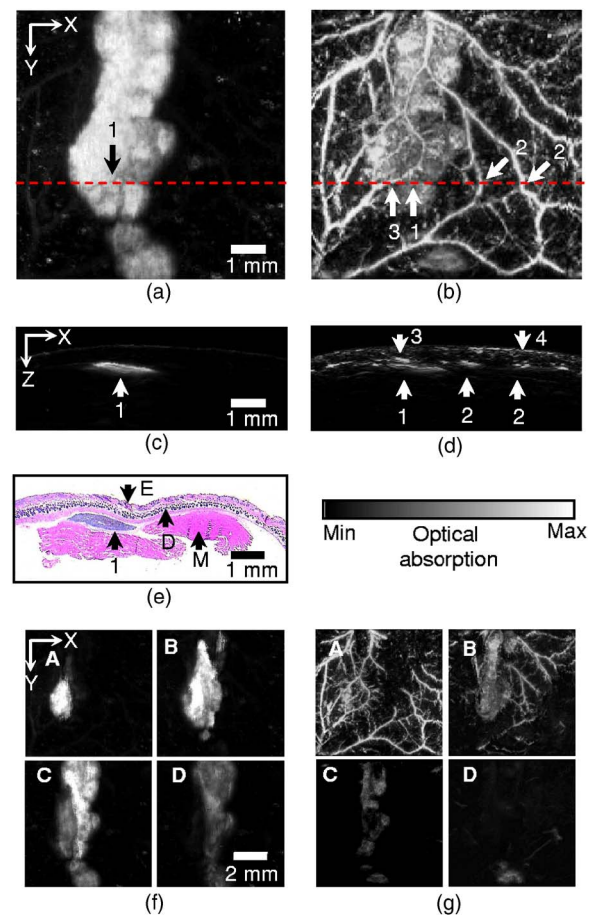


Fig. 3 *In vivo* noninvasive photoacoustic images of melanoma and vascular distribution in nude mouse skin. (a),(b) Enface photoacoustic images for the NIR light source ($\lambda=764\text{ nm}$) and visible light source ($\lambda=584\text{ nm}$), respectively: 1, melanoma; 2, vessels perpendicular to image plane; 3, vessels horizontal to image plane; 4, skin. (c),(d) Photoacoustic B-scan images from the NIR and visible light sources, respectively, for the dot lines in (a) and (b). (e) A cross-sectional histology image (H&E staining): E, epidermis; D, dermis; M, muscle. (f),(g) Depthwise enface photoacoustic images from the NIR and visible light sources, respectively; A, 0.15–0.30 mm; B, 0.30–0.45 mm; C, 0.45–0.60 mm; D, 0.60–0.75 mm from the skin surface.

arterial blood oxygenation were monitored during the entire experiment using a pulse oximeter (Model 8600, Nonin Medical Inc.) After imaging, the mice were sacrificed using pentobarbital (120 mg/kg, IP). The imaged melanoma and surrounding tissue were excised and stained with hematoxylin and eosin (H&E) for histology. All of the experimental animal procedures were approved by the University Laboratory Animal Care Committee of Texas A&M University.

Figure 3 shows the *in vivo* photoacoustic image of a subcutaneous melanoma and the surrounding vascular distribution in nude mouse skin. Three-dimensional images of the subcutaneous melanoma were obtained. Figures 3(a) and 3(b) show maximum intensity projection images that are like enface images (160×160 pixels; $50\text{-}\mu\text{m}$ step size) from the NIR and visible light sources, respectively. The images are gray-level plots of the maximum amplitude of the signal envelope of the received photoacoustic signals within the skin to the entire measurement depth versus the 2-D transducer posi-

tions. The melanoma is indicated by arrow 1 in both images. The photoacoustic image that was obtained with NIR light shows only the melanoma, but the photoacoustic image that was acquired with visible light shows both the melanoma and the blood vessels as indicated by arrows 2 and 3. The high selectivity for the melanin pigmented melanoma is caused by the large difference in the absorption coefficients of NIR light in melanin and in blood. With NIR light, the absorption ratio between melanin and blood cannot be measured exactly from the image because the photoacoustic signals from the blood vessels are far below the noise level of the system. With visible light, photoacoustic signals from the blood vessels are around 1.5 to 2.5 times higher than those from the melanoma.

Figures 3(c) and 3(d) are photoacoustic cross-sectional images obtained along the dotted lines shown in Figs. 3(a) and 3(b). Each image is a gray-scale plot of the envelope magnitude of the received photoacoustic signals. The vertical axis and the horizontal axis represent, respectively, the depth from the skin and the horizontal transducer position, and each image has a physical size of 3.0 mm in depth and 8.0 mm in width. The arrows in the images correspond to those in the projection images. Note that the signal from the bottom of the melanoma is clearly seen in the NIR image, which allows us to measure the thickness of the melanoma. The maximum thickness and depth of the subcutaneous melanoma are found to be 0.3 and 0.45 mm, respectively. Normalizing the signal from the lower boundary with the upper one allows us to compare the signal decay of the *in vivo* data with the melanoma phantom results in Fig. 2(b). The normalized values of the lower boundary signals from the *in vivo* experiment indicate a signal decay of 50% to 60%, which is close to the values of 40% to 60% for the 0.25-mm-thickness phantom cases. In the visible light image, the detection of the thickness is impeded by ambiguity in the determination of melanin from blood due to their similar absorption coefficients as well as the weak signal from the bottom. For comparison, Fig. 3(e) shows a histological cross-sectional image of the skin containing a melanoma within the subcutaneous tissue (H&E staining) for the corresponding photoacoustic images. Good agreement in the morphology of the melanoma is observed between the photoacoustic image and the histologic image in terms of size and depth.

Figures 3(f) and 3(g) show multiple maximum intensity projection images for several depths from the skin surface for both light sources. By projecting the signal envelope amplitude of the received signal within certain depths, depthwise enface images of the melanoma and the vascular anatomy surrounding it were found. These images reveal that the melanoma has a complex 3-D shape, and the maximum thickness and depth from the skin surface are found to be 0.5 and 0.15 mm, respectively. By imaging the entire shape of the melanoma, a true thickness profile, which is difficult to obtain from a single B-scan image, can be acquired. The vascular system is found to be located between 0.15 to 0.45 mm from the skin surface, where dermis lies. Some of the blood vessels surrounding the melanoma are believed to be feeding vessels.¹² Because the anatomy of the vascular system is important for determining tumor invasiveness, visible light im-

ages can be used for diagnostic and prognostic purposes as well.

Using dark-field illumination mode photoacoustic microscopy with a pair of pulsed lasers whose wavelengths were selected based on the large absorption difference between blood and melanoma, 3-D structures of subcutaneous melanoma were imaged. Currently, the imaging speed is limited by the pulse repetition rate of the lasers that we used. Even without averaging, it takes about 65 min with a laser repetition rate of 10 Hz to image an 8- × 8-mm area. This time doubles for imaging at both wavelengths. Because lasers with a pulse repetition rate of 1 kHz are now available on the market, it is possible to reduce the imaging time significantly. In order to apply this technology to clinical situations, the capability to increase the maximum measurable thickness of a melanoma is also important. The current results indicate that the maximum thickness is determined by the light absorption distribution and the system SNR. Thus, further improvement is possible by optimizing the dark-field illumination angle for thick melanomas and reducing the ultrasonic frequency in order to increase the image depth. We expect that this technology will contribute to the imaging of skin tumors.

Acknowledgments

This research was supported in part by the National Institutes of Health grants R01 EB000712 and R01 NS46214. J. T. Oh was supported in part by the postdoctoral Fellowship Program of Korea Science & Engineering Foundation (KOSEF).

References

1. R. T. Greenlee, T. Murray, and S. Bolden, "Cancer statistics, 2000," *Ca-Cancer J. Clin.* **50**, 7–33 (2000).
2. W. H. Clark, Jr., A. M. Anisworth, E. A. Bernardino, C. Yang, M. C. Mihm, and R. J. Reed, "The development biology of primary human malignant melanoma," *Semin. Oncol.* **2**, 88–103 (1975).
3. H. Pehamberger, M. Binder, A. Steiner, and K. Wolff, "In vivo epifluorescence microscopy: improvement of early diagnosis of melanoma," *J. Invest. Dermatol.* **100**, 356–362 (1993).
4. M. Rajadhyaksha, M. Grossman, D. Esterowitz, R. H. Webb, and R. R. Anderson, "In vivo confocal scanning laser microscopy of human skin: melanin provides strong contrast," *J. Invest. Dermatol.* **104**, 946–952 (1995).
5. P. Altmeyer, S. El-Gammal, and K. Hoffmann, *Ultrasound in Dermatology*, Springer-Verlag, Berlin (1992).
6. X. Wang, Y. Pang, G. Ku, X. Xie, G. Stoica, and L. V. Wang, "Non-invasive laser-induced photoacoustic tomography for structural and functional *in vivo* imaging of the brain," *Nat. Biotechnol.* **21**, 803–806 (2003).
7. K. Maslov, G. Stoica, and L. V. Wang, "In vivo dark-field reflection-mode photoacoustic microscopy," *Opt. Lett.* **30**, 625–627 (2005).
8. S. Jacques and D. McAuliffe, "The melanosome: threshold temperature for explosive vaporization and internal absorption coefficient during pulsed laser irradiation," *Photochem. Photobiol.* **53**, 769–775 (1991).
9. *American National Standard for the Safe Use of Lasers, ANSI Standard Z136*, American National Standards Institute, New York (2000).
10. M.-L. Li, H. F. Zhang, K. Maslov, G. Stoica, and L. V. Wang, "Improved *in vivo* photoacoustic microscopy based on a virtual detector concept," *Opt. Lett.* **31**, 474–476 (2006).
11. L. Wang, S. L. Jacques, and L. Zhang, "MCML-Monte Carlo modeling of photon transport in multi-layered tissues," *Comput. Methods Programs Biomed.* **47**, 131–146 (1995).
12. G. Ku, X. Wang, X. Xie, G. Stoica, and L. V. Wang, "Imaging of tumor angiogenesis in rat brains *in vivo* by photoacoustic tomography," *Appl. Opt.* **41**, 770–775 (2005).